Available online at www.sciencedirect.com

SciVerse ScienceDirect

Ceramics International 39 (2013) 3901–3907

CERAMICS INTERNATIONAL

www.elsevier.com/locate/ceramint

Physical properties of spray deposited Ni-doped zinc oxide thin films

S.K. Patil, S.S. Shinde, K.Y. Rajpure*

Electrochemical Materials Laboratory, Department of Physics, Shivaji University, Kolhapur 416004, India

Received 3 October 2012; received in revised form 20 October 2012; accepted 21 October 2012
Available online 5 November 2012

Abstract

Transparent thin films of nickel doped zinc oxide were deposited on to corning glass substrates via chemical spray pyrolysis using zinc acetate and nickel nitrate as precursors. Structural, morphological, optical, electrical, dielectrical and impedance properties of the films as a function of nickel doping concentration as well as inter-particle interactions by complex impedance spectroscopy were investigated. The deposited films are polycrystalline with a hexagonal (wurtzite) crystal structure along (002) preferential orientation. The films are highly transparent in the visible region with a transmittance higher than 86%, and have an optical band gap ranging from 3.23 to 3.19 eV depending on the nickel doping concentration. The high electrical conductivity of doped films is explained on the basis of the presence of oxygen vacancies. Decrease of electrical conductivity due to nickel doping is explained on the basis of compensation of oxygen vacancies. The dielectric constant and loss tangent as a function of frequency are reported. Interparticle interactions in the deposited films are studied by complex impendence spectroscopy.

Keywords: Ni:ZnO; XRD; Optoelectronic properties; Impendence

1. Introduction

Zinc oxide is an attractive semiconductor for numerous applications and a building block material for optoelectronic devices because of its large band gap (3.3 eV), exciton binding energy (60 meV), transparency, chemical stability, etc. It has tremendous applications such as LEDs, transparent FETs, photodetectors [1–3], spintronics and piezoelectric devices [4,5]. However, these applications are mostly dependent on intrinsic defects or additional defects [6]. The physical properties of semiconductors are efficiently enhanced by incorporating impurity doping. ZnO is usually n-type due to electron doping via defects originating from Zn interstitials and O vacancies in the lattice. The understanding of the role of various impurities and defects in ZnO lattice is very crucial.

Yan et al. [7] reported synthesis and optical properties of Mn and Ni-doped ZnO thin films by sol–gel process in methyl alcohol. The effect of Ni concentration on the structural, electrical, optical, and non-linear optical properties of the Ni:ZnO thin films was investigated by Abed et al. [8]. The effective non-linear quadratic and cubic electronic susceptibilities of thin films were also determined by the SHG and THG techniques. Liu et al. [9] reported the growth of Ni-doped ZnO ($Zn_{1-x}Ni_xO$) thin films on quartz substrates via magnetron sputtering process with the Ni concentrations of 5, 10 and 20 at%. Pandey et al. [10] reported the synthesis of a transparent magnetic semiconductor by incorporating Ni in zinc oxide matrix prepared by fast atom beam (FAB) sputtering. They discussed an interaction between free charges generated by doping and localized d spins of Ni. Combining optical properties (high transmittance) with the electrical conductivity and magnetic behavior of Ni-doped ZnO is of enormous consequence in the field of transparent spintronic devices. Therefore, a detailed study on the transport and optical transmission is required for better understanding of this material. These films have been prepared by a variety of techniques like sol–gel [7], magnetron sputtering [9], Fast atom beam sputtering [10], Pulsed laser deposition [11], Chemical vapor deposition [12] and spray pyrolysis

*Corresponding author. Tel.: +91 231 2609435; fax: +91 231 2691533.
E-mail address: rajpure@yahoo.com (K.Y. Rajpure).

0272-8842/$ - see front matter © 2012 Elsevier Ltd and Techna Group S.r.l. All rights reserved.
http://dx.doi.org/10.1016/j.ceramint.2012.10.234

[13,14]. Among many techniques, spray pyrolysis plays an important role on microstructures, optical, electrical and magnetic properties of the materials.

Many authors have extensively investigated Ni-doped ZnO thin films by spray pyrolysis [13,14]. However, all of them used a mixture of water, acids, methanol and ethanol as solvents for preparing the spraying solution. Considering the need for the environmental affability of the deposition technique, acids and alcohols are harmful and toxic gases are evolved during pyrolytic decomposition of the spraying solution in the spray technique. Combining optical properties (better transparency) with an electrical conductivity and magnetic behavior of Ni-doped ZnO is of enormous consequence in the field of transparent spintronic devices. Therefore, a meticulous study on the transport and optical properties is necessary for better understanding of this material. In this work, we have studied nickel-doped ZnO thin films in the perception of their transparent and electrically conducting properties. The influence of Ni doping on to structural, morphological, optical, electrical, dielectrical and impedance properties of zinc oxide host lattice has been investigated.

2. Experimental

ZnO thin films were grown by chemical spray pyrolysis onto corning glass substrates using zinc acetate [$Zn(CH_3COO)_2 \cdot 2H_2O$] as a precursor. The precursor solution was prepared from a mixture of 0.1 M [$Zn(CH_3COO)_2 \cdot 2H_2O$] 99.99%, A.R. Grade, Himedia dissolved in double distilled water. To obtain doped ZnO thin films with nickel was added in solution by using $Ni(NO_3).6H_2O$ compound. The atomic percentages of [Ni/Zn] were 0.5, 1.0, 1.5, 2.0 and 2.5 at% respectively. It was observed that for higher doping concentration degradation of films occurs probably due to a reaction of the solution with excess nickel. The actual [Ni]/[Zn] ratios in the film are far less than in the solution. Before loading into the system, the substrates were washed with detergent and then completely rinsed in methanol; acetone and double distilled water and finally dried in air. Then the substrates were progressively heated up to the required temperature, before being sprayed on. The resulting solution was sprayed onto the preheated substrates held at optimized substrate temperature of 450 °C [15]. Compressed air was used as a carrier gas. Other preparative parameters, such as spray rate (5 cm^3/min), distance between the atomizer and the substrates (30 cm) were kept constant for all experiments.

The structural characterization of deposited thin films was carried out, by analyzing the X-ray diffraction patterns obtained under Cr–Kα radiation from a Philips X-ray diffractometer model PW-3710 and surface morphology was studied using a scanning electron microscope, JEOL JSM-6360, Japan. Transmission spectra were recorded at room temperature and near to normal incidence using a 119 SYSTRONICS UV–Vis spectrophotometer. Resistivity measurements were carried out by two probe method as a function of temperature. The type of semiconductor was examined from thermoelectric power (TEP) measurement. The AC parameters such as capacitance (C) and dissipation factor (tan δ) of the films were measured in the frequency range from 20 Hz to 1 MHz using an LCR meter (HP 4284 A). The dielectric constant (ε') was calculated using the relation [16].

3. Results and discussion

3.1. Structural analysis

X-ray diffraction (XRD) patterns of Ni-doped ZnO (NZO) thin films for different Ni doping concentrations from 0.5 to 2.5 at% at optimized substrate temperature 450 °C are shown in Fig. 1. A matching of the observed and standard '*d*' values of NZO using JCPDS card no. 05-0664 confirms the deposited films fit well with the hexagonal (wurtzite) crystal structure having preferred orientation along (002) plane. The intensity of (002) plane increases while the intensity of (101) plane decreases up to 1.5 at% and vice versa, showing crystal reorientation effect [17]. Relatively prominent ZnO (002) peaks are attributed to the lower levels of Ni content in the films and also attributed to the Ni^{2+} ions which is substituted for the Zn^{2+} ions to form the primary phase Ni^{2+}:ZnO. Some weak reflections such as (102) and (103) have also been observed but with smaller intensities. No peaks corresponding to metallic Zn or Ni are observed in the XRD patterns. The average crystallite size of ZnO thin films is calculated using the Scherrer's relation [17]. The crystallite size enhances with doping concentration up to 1.5 at% and then decreases as seen in Fig. 2. The average crystallite size of the NZO thin films varies from 30 to 36 nm. The dopant atom destroys the initial preferential

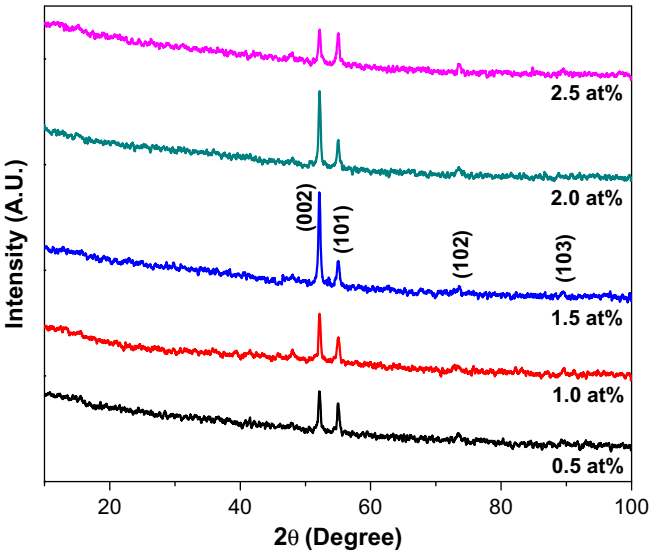

Fig. 1. X-ray diffraction patterns of Ni-doped zinc oxide thin films for different doping concentrations.

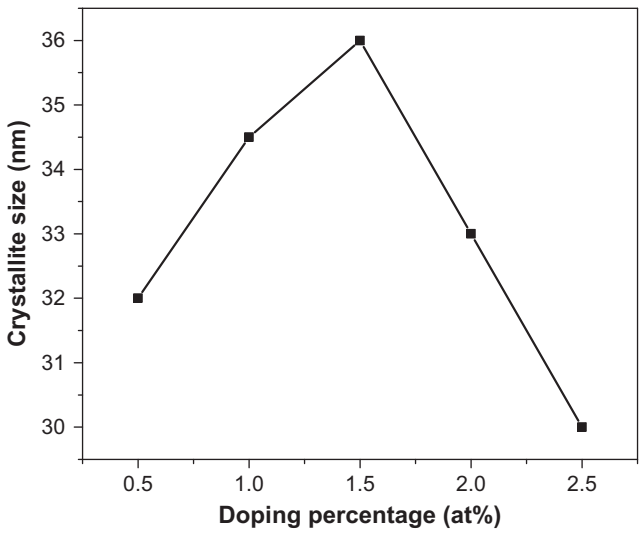

Fig. 2. Variation of crystallite size with Ni doping concentration.

orientation of the host lattice with increasing doping concentration while it becomes polycrystalline with vanishing textured structure. It is obvious that the Ni doping modifies the growth mechanism. As seen, the growth rate increases linearly with increasing the doping level. It is worth noting that the (002) plane requires lower energy formation. Therefore, growth rate becomes faster with increase in Ni doping concentration; consequently the easiest formation of (002) plane is favored.

3.2. Morphological analysis

Fig. 3 shows the SEM images of Ni-doped ZnO thin films. All the films are homogeneous, dense, adherent and grow with thin columnar grains perpendicular to the substrate. It is apparent that the morphology of the films has tightly packed grains and relatively smooth surfaces without any voids and crack. Apparently hexagonal-shaped granules are seen without any noticeable pinholes, which are uniformly distributed, giving a smooth surface morphology. The grain size slightly decreases with increasing the Ni content up to 1.5 at% and then increases. It is attributed to the impurity effect of Ni on film structure. i.e., large number of Ni atoms as impurity can lead to a high nucleation density at initial stage of film growth, decreasing grain size of the film.

3.3. Optical properties

Fig. 4 shows the optical transmittance spectra of NZO thin films deposited at various Ni doping concentrations. They show strong interference fringes due to the multiple reflections at the interfaces; their observation indicates a fairly homogeneous film thickness. All these films show higher transparency in the visible range with an average transmittance of about 85%. The transmittance falls sharply at the band edge which is an indication of the good films crystallinity. Besides, the absorption edge of NZO films deposited for different doping concentration shifts to a larger wavelength. This phenomenon indicates that the optical energy gap is decreased with doping concentration. For a direct band gap semiconductor, the optical band gap energy (E_g) can be estimated from the absorption spectrum using to the following relation [18]:

$$\alpha h\nu = C\left(h\nu - E_g\right)^{1/2} \quad (1)$$

Optical energy gap (E_g) of the films is obtained by extrapolating linear part of the spectrum $(\alpha h\nu)^2$ vs. ($h\nu$) to zero. We observed that the band gap of NZO films decreases with Ni concentration from 3.23 to 3.19 eV.

3.4. Electrical properties

Fig. 5 shows the variation of $\ln \rho$ against $(1000/T)$ for Ni-doped ZnO thin films. It is well known that the film microstructure plays an important role in the electrical properties of the semiconductors. The decrease in dc electrical resistivity with increasing temperature confirms the semiconducting behavior of NZO thin films. It is seen that electrical resistivity decreases with Ni doping concentration up to 1.5 at% and then increases for higher doping concentration. It is due to the fact that nickel exceeds the maximum limit of solubility in zinc oxide, producing a grain boundary segregation of impurities that causes a dispersion of carriers. The XRD patterns indicate that the increase of crystallite size results in decrease of grain boundaries leading to enhancement in conductivity. However, when the Ni doping ratio exceeds 1.5 at% the conductivity decreases. The higher c-axis preferred orientation results in higher conductivity because of the reduction in the scattering of the carries at the grain boundaries [19]. For analysis of defect levels generated in the samples, the activation energy is calculated by using the relation [16]

$$\rho = \rho_0 \exp\left(\frac{E_a}{kT}\right) \quad (2)$$

where E_a is the activation energy, ρ the resistivity at room temperature, k the Boltzmann constant and ρ_0 is the temperature independent constant. Fig. 6 depicts the variation of activation energy with Ni doping concentration. It shows that, as the doping concentration increases up to 1.5 at% the activation energy decreases showing lowest value 0.2979 eV and then increases. It is remarkable that the activation energy increases due to grain relaxation with porosity. The activation energy shows the position of the Fermi level compared to that of the conduction band.

3.5. Thermoelectric power

The type of conductivity exhibited by NZO thin films is determined from thermoelectric power analysis. The polarity of thermally generated voltage at the cold end is negative which confirms the films are of n-type. Fig. 7 shows the variation of thermo-emf against temperature difference for the films deposited at different Ni doping concentrations. It is

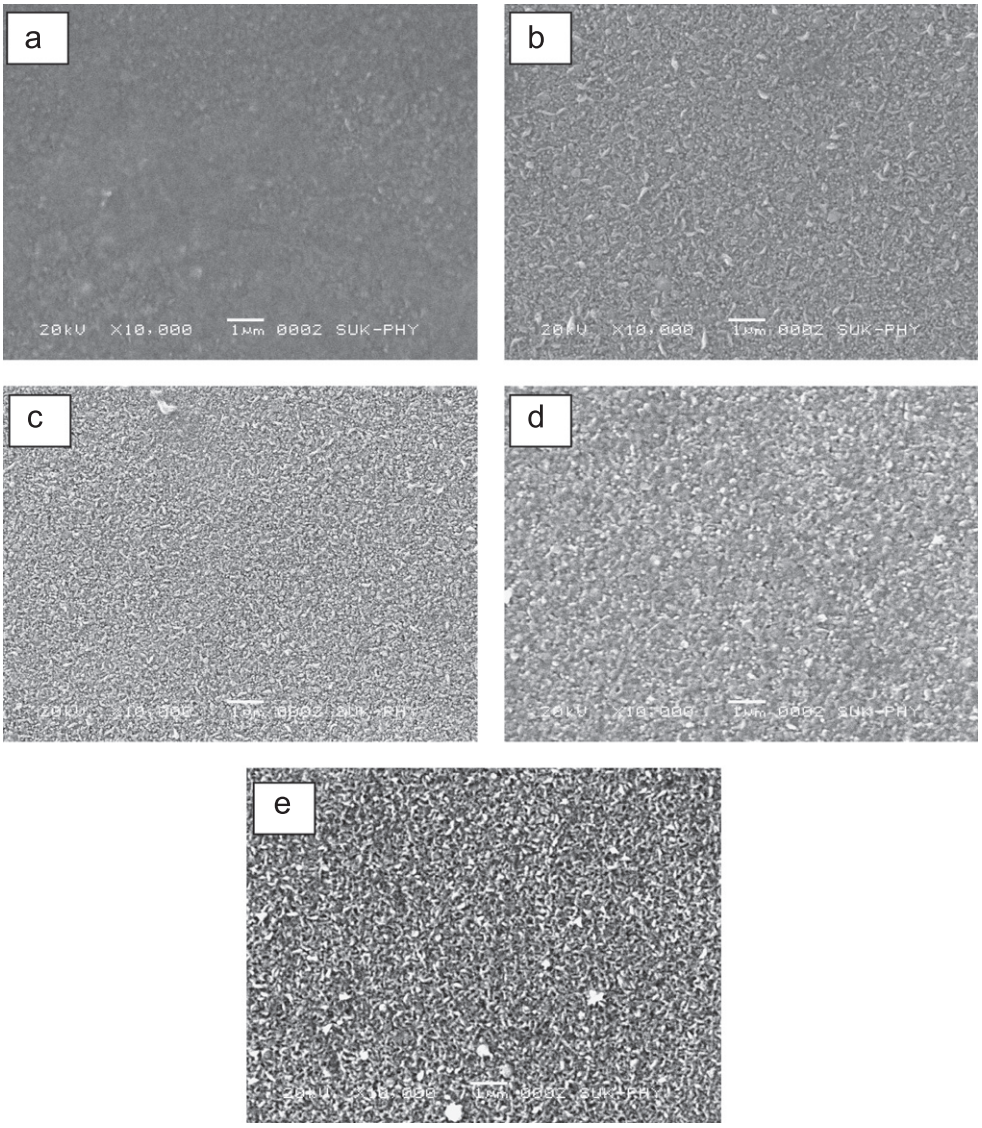

Fig. 3. Scanning electron micrographs of Ni-doped zinc oxide thin films: (a) 0 at%, (b) 0.5 at%, (c) 1.0 at%, (d) 1.5 at%, (e) 2.0 at% and (f) 2.5 at%.

found that, the thermo-emf increases with doping concentration up to 1.5 at% and then decreases for higher doping concentrations and it varies linearly with difference in temperature. Relatively higher thermo-emf is observed for the film deposited at 1.5 at% doping concentration is due to better crystallinity. The location of Fermi energy and the type of scattering mechanism in the material decides the Seebeck coefficient. Seebeck coefficient increases as the Fermi energy moves further into the energy gap from the bottom edge of conduction band.

3.6. Dielectric properties

The variation of dielectric constant with respect to frequency at room temperature is shown in Fig. 8. It is seen that the dielectric constant (ε') decreases suddenly at lower frequencies and remains constant at higher frequencies, showing the dispersion behavior of dielectric constant at lower frequencies owing to the charge transport relaxation time. The dielectric constant increases up to 1.5 at% Ni doping and then decreases. The large value of the dielectric constant (2.6 at 1000 Hz) is associated with space charge polarization and inhomogeneous dielectric structure viz. impurities, grain structure, defects and pores. The decrease in dielectric constant takes place when jumping frequency of electric charge cannot follow the change in applied electric field beyond a certain critical frequency. Decrease in dielectric constant with frequency is due to decrease in polarization. At lower frequencies, dielectric loss, $\tan\delta$, (Fig. 9) is large and it decreases with increasing frequency. $\tan\delta$ is the energy dissipation in the dielectric system, which is proportional to the imaginary part of the dielectric constant. An increase in loss factor at higher frequencies is may be due to the series resistance of the electrodes [20]. The appearance of minimum loss with

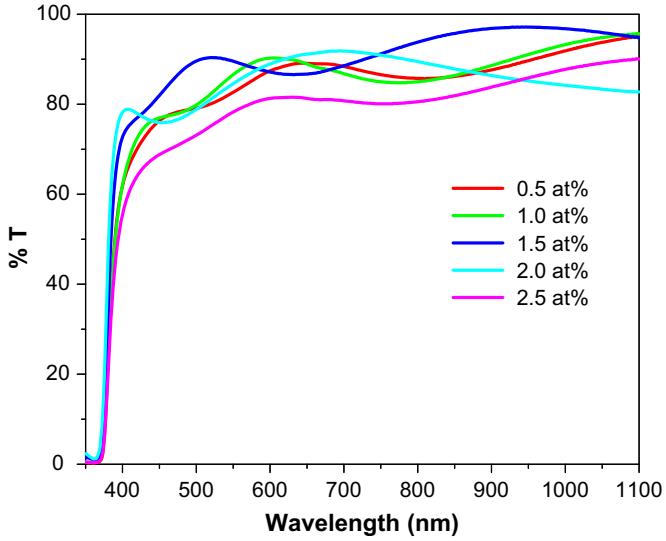

Fig. 4. Optical transmittance spectra of Ni-doped zinc oxide thin films.

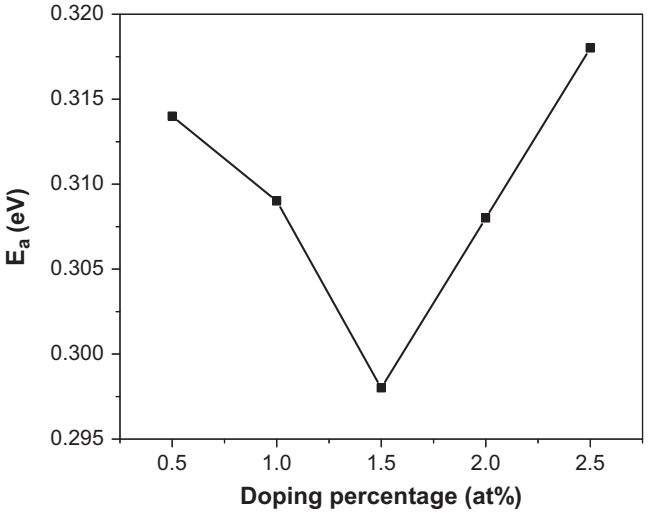

Fig. 6. The variation of activation energy with Ni doping concentration.

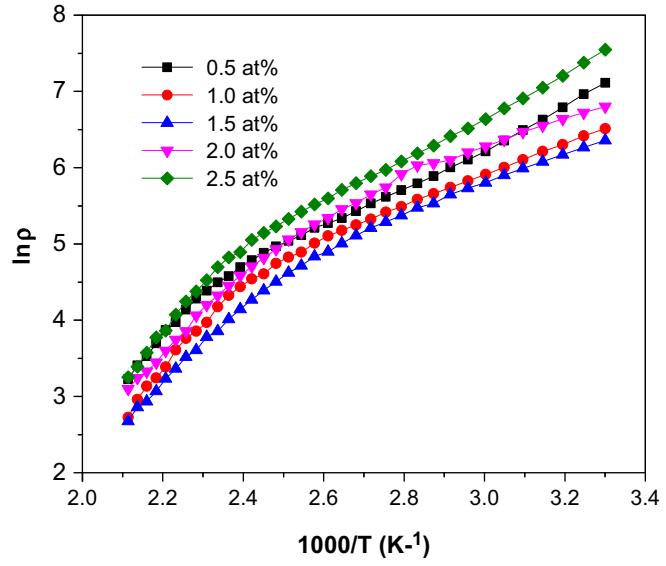

Fig. 5. Variation of resistivity with respect to temperature for Ni-doped zinc oxide thin films.

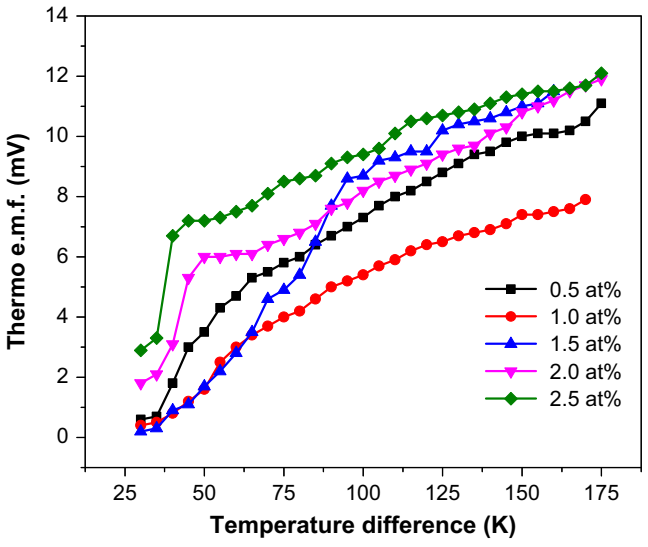

Fig. 7. The variation of thermo emf. with Ni doping concentration.

frequency is a direct consequence of a mathematical analysis of an equivalent capacitance circuit for oxide dielectric films [21]. The higher values of dielectric constant and loss tangent observed at 1.5 at% Ni are due to the large surface charge sorption of the Ni^{2+} ion in ZnO host lattice.

3.7. Impedance analysis

Fig. 10 represents the real (Z_r) and imaginary component (Z_i) in the complex plan for Ni-doped ZnO thin films at room temperature. The center of the semicircle is localized below the real axis attributed to a constant phase element. The impedance spectrum is characterized by the appearance of semicircle arcs whose pattern changes, but not its shape, when the doping concentration is increased. Such pattern tells us about the electrical process occurring within the film and their correlation with their microstructures. Intersect with real axis of the semicircle at low frequency is attributed to the total resistance RT. On the other hand, the impedance response of grain governs at high frequencies and the resistance of grain is deduced from the left intersect of the semicircle with real axis. The intercept of semicircle with real axis at low frequency represents the sum of the resistance of grains and grain boundaries, while the intercept at high frequency represents the resistance of grains only. Grain boundary resistance decreases with doping concentration up to 1.5 at% and then increases, it seems that grain boundary effect has assisted in lowering the barrier to the motion of charge carriers. The impedance value is typically higher at lower temperatures in the low-frequency region and decreases gradually with increasing frequency. Also Z' decreases with doping concentration up to 1.5 at% indicating an increase in conductivity as confirmed from electrical measurements.

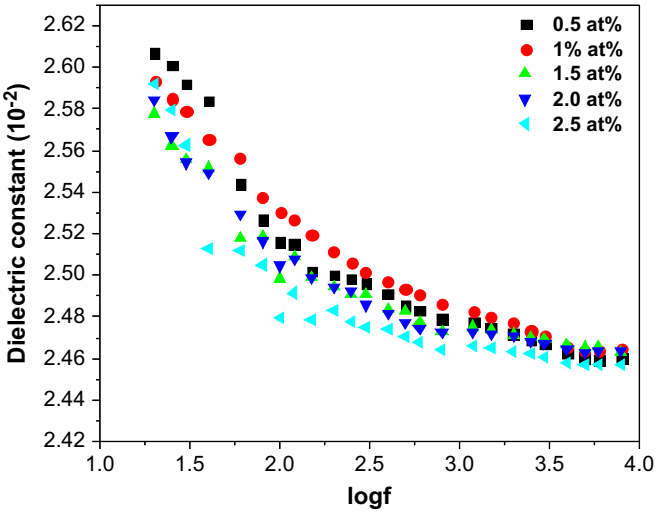

Fig. 8. The variation of dielectric constant with Ni doping concentration.

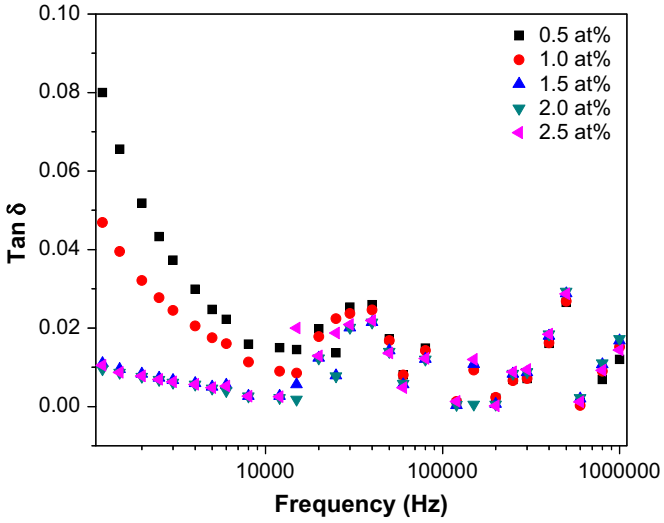

Fig. 9. The variation of loss tangent with Ni doping concentration.

4. Conclusions

The transparent Ni-doped ZnO thin films were successfully prepared by spray pyrolysis in an aqueous medium. Structural analysis shows that the pure and Ni-doped ZnO films are polycrystalline with a hexagonal (wurtzite) crystal structure. The observed highest visible range transmittance is about 80–85%. The dielectric behavior shows the electronic polarizability at higher frequencies due to space charge polarization.

Acknowledgments

Authors are very much thankful to UGC and DST for the financial support through UGC-DSA-I, DST-PURSE and DIST-FST-II programmes.

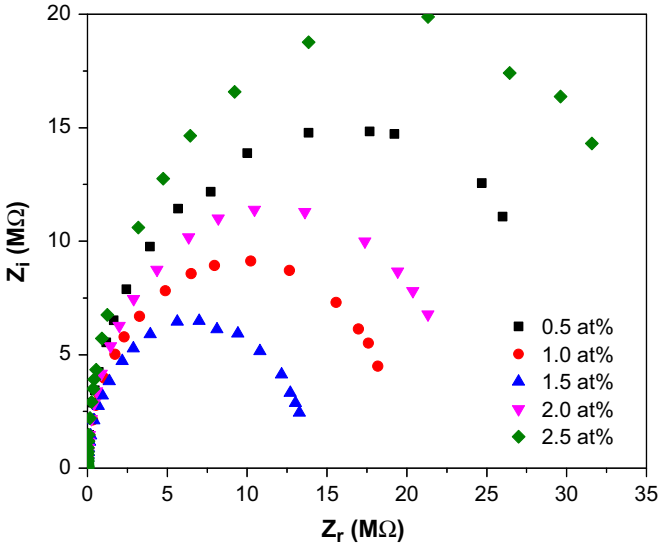

Fig. 10. Complex impedance spectra of Ni-doped zinc oxide thin films.

References

[1] S. Liang, H. Sheng, Y. Liu, Z. Huo, Y. Lu, H. Shen, ZnO Schottky ultraviolet photodetectors, Journal of Crystal Growth 225 (2001) 110–113.

[2] S.S. Shinde, K.Y. Rajpure, Fabrication and performance of N-doped ZnO UV photoconductive detector, Journal of Alloys and Compounds 522 (2012) 118–122.

[3] S.S. Shinde, K.Y. Rajpure, Fast response ultraviolet Ga-doped ZnO based photoconductive detector, Materials Research Bulletin 46 (2011) 1734–1737.

[4] S. Saleh, H. Elsimary, A. Zaki, S. Ahmed, Design and fabrication of piezoelectric acoustic sensor, WSEAS Transaction on Electronics 3 (2006) 192–196.

[5] U. Ozgur, Y.I. Alivov, C. Liu, A. Teke, M.A. Reshchikov, S. Dogan, V. Vrutin, S.J. Cho, H. Morkoc, A comprehensive review of ZnO materials and devices, Journal of Applied Physics 98 (2005) 041301.

[6] L. Schmidt-Mende, J.L. ManManus-Driscoll, ZnO—nanostructures, defects, and devices, Materials Today 10 (2007) 40–48.

[7] Xiaolu Yan, Dan Hu, Hangshi Li, Linxiao Li, Xiaoyu Chong, Yude Wang, Nanostructure and optical properties of M doped ZnO (M= Ni, Mn) thin films prepared by sol–gel process, Physica B 406 (2011) 3956–3962.

[8] S. Abed, M.S. Aida, K. Bouchouit, A. Arbaoui, K. Iliopoulos, B. Sahraoui, Non-linear optical and electrical properties of ZnO doped Ni thin films obtained using spray ultrasonic technique, Optical Materials 33 (2011) 968–972.

[9] E. Liu, P. Xiao, J.S. Chen, B.C. Lim, L. Li, Ni doped ZnO thin films for diluted magnetic semiconductor materials, Current Applied Physics 8 (2008) 408–411.

[10] B. Pandey, S. Ghosh, P. Srivastava, D.K. Avasthi, D. Kabiraj, J.C. Pivin, Synthesis and characterization of Ni-doped ZnO: a transparent magnetic semiconductor, Journal of Magnetism and Magnetic Materials 320 (2008) 3347–3351.

[11] J.C. Pivin, G. Socol, I. Mihailescu, P. Berthet, F. Singh, M.K. Patel, L. Vincent, Structure and magnetic properties of ZnO films doped with Co, Ni or Mn synthesized by pulsed laser deposition under low and high oxygen partial pressures, Thin Solid Films 517 (2008) 916–922.

[12] Z. Shao Min, Y. Hong Lei, L. Li Sheng, C. Xi Liang, L. Shi Yun, H. Yao Ming, Y. Rui Jian, L. Ning, Magnetic properties of Ni-doped ZnO nanocombs by CVD approach, Nanoscale Research Letters 5 (2010) 1284–1288.

[13] H. Benzarouk, A. Drici, M. Mekhnache, A. Amara, M. Guerioune, J.C. Bernède, H. Bendjffal, Effect of different dopant elements (Al, Mg and Ni) on microstructural, optical and electrochemical properties of ZnO thin films deposited by spray pyrolysis (SP), Superlattices Microstructure 52 (2012) 594–604.
[14] A. Maldonado, S. Tirado-Guerra, M. dela L. Olvera, Chemically sprayed ZnO:(F, Zr) thin films: effect of starting solution ageing time and substrate temperature on the physical properties, Journal of Physics and Chemistry of Solids 70 (2009) 571–575.
[15] S.S. Shinde, P.S. Shinde, R.T. Sapkal, Y.W. Oh, D. Haranath, C.H. Bhosale, K.Y. Rajpure, Photoelectrocatalytic degradation of oxalic acid by spray deposited nanocrystalline zinc oxide thin films, Journal of Alloys and Compounds 538 (2012) 237–243.
[16] V.S. Sawant, S.S. Shinde, R.J. Deokate, C.H. Bhosale, B.K. Chougule, K.Y. Rajpure, Effect of calcining temperature on electrical and dielectric properties of cadmium stannate, Applied Surface Science 255 (2009) 6675–6678.
[17] S.S. Shinde, C.H. Bhosale, K.Y. Rajpure, Structural, optical, electrical and thermal properties of zinc oxide thin films by chemical spray pyrolysis, Journal of Molecular Structure 1021 (2012) 123–129.
[18] J.I. Pankove, Optical Processes in Semiconductors, Dover, New York, 1976.
[19] K.T. Kim, G.H. Kim, J.C. Woo, C. Kim, Characteristics of nickel-doped zinc oxide thin films prepared by sol–gel method, Surface and Coatings Technology 202 (2008) 5650.
[20] A. Goswami, A.P. Goswami, Dielectric and optical properties of ZnS films, Thin Solid Films 16 (1973) 175.
[21] I.H. Pratt, S.J. Firestone, Fabrication of RF-sputtered barium titanate thin films, Journal of Vacuum Science and Technology 8 (1971) 256.